© 2023 The Authors
Published by the European Association of Geochemistry

Authigenic minerals reflect microbial control on pore waters in a ferruginous analogue

A. Vuillemin, M. Morlock, A. Paskin, L.G. Benning, C. Henny, J. Kallmeyer, J.M. Russell, H. Vogel

Supplementary Information

The Supplementary Information includes:

- Supplementary Methods
- Figures S-1 to S-8
- Table S-1
- Supplementary Information References

Supplementary Methods

Core recovery, water column profiles, gravity cores

The oxygen concentration profile was collected on site using a submersible conductivity-temperature-depth probe (Sea-Bird SBE-19, Sea-Bird Electronics). The Fe^{2+} concentration profile was obtained from water samples (Bauer *et al*., 2020) collected using 5 L Niskin bottles (General Oceanics) attached in series and placed at depth using a commercial FCV 585 fish finder (Furuno Electric Co.). The upper 0.35 m of the sediment record corresponds to samples obtained *via* short gravity coring during pilot campaigns in November 2013 and 2014, and sampled as described in Vuillemin *et al*. (2016), whereas the 100-m-long sediment sequence comes from hydraulic cores obtained as part of the Towuti Drilling Project (TDP).

The TDP coring operations were carried out from May to July 2015 using the International Continental Scientific Drilling Program (ICDP) Deep Lakes Drilling System (Russell *et al*., 2016). Hole TDP-1A (156 m water depth) was drilled in May 2015 with a fluid contamination tracer added to the drill mud prior to operations and used to aid geomicrobiological sampling and analysis. All core sections were checked for contamination and those containing the tracer were discarded (Friese *et al*., 2017). Samples were collected from TDP-1A cores immediately upon recovery and were subsequently cut from the core sections into 5 and 10 cm long whole round cores (WRC), 6.6 cm in diameter, immediately capped and transferred to an anaerobic chamber flushed with nitrogen to avoid oxidation during sample handling, and processed in the field for analyses of pore water chemistry, cell count and microbial DNA fingerprinting.

In January 2016, the unsampled remainders of TDP-1A cores were split and scanned at the Limnological Research Center, Lacustrine Core Facility (LacCore), University of Minnesota, described macroscopically and microscopically to determine their stratigraphy and composition (Russell *et al*., 2016), then subsampled for dense mineral extraction (Vuillemin *et al*., 2019a).

Bulk analyses

Total organic carbon (TOC) was determined as the difference between elemental analyser (Total Carbon) and coulometric (Total Inorganic Carbon) analyses (Russell *et al*., 2020). Coulometric measurements were carried out at 60 °C with H_2SO_4 and a reaction time of 20 min. Siderite concentrations in bulk sediments were calculated based on mineral carbon values (MinC %) obtained from previous Rock-Eval analyses and corrected according to published equations of linear regression (Ordoñez *et al*., 2019). Results for siderite concentrations based on coulometric and Rock-Eval analyses were consistent, with about 20 % siderite in red clays at depth in the sediment succession.

For iron speciation, a subsample of 500 mg of wet sediment from each core interval of both sediment cores was extracted in the field and immediately leached in 1 mL 0.5 N HCl, and Fe-speciation (Fe^{II} and Fe^{III}) of the easily extractable Fe-phases was measured spectrophotometrically on site using a ferrozine assay (Viollier *et al*., 2000). For reactive and total Fe sequential extraction, the complete Fe-speciation protocol was performed on anoxically preserved and freeze-dried sediments milled to fine powders using an agate hand mortar and pestle. Sample masses of 200 mg of sediment were processed following the protocol described in (Poulton and Canfield, 2005). The highly reactive Fe pool is defined as the sum of hydrous Fe (oxyhydr)oxides including ferrihydrite and lepidocrocite (0.5 N HCl extractable Fe), carbonate-associated Fe (acetate extractable Fe), ferric (oxyhydr)oxides including hematite and goethite (dithionite extractable Fe), and magnetite ($Fe^{2+}Fe_2{}^{3+}O_4$) (oxalate extractable Fe). These reagents do not extract the Fe present in pyrite ($Fe^{2+}S_2$) (Henkel *et al*., 2018). The non-reactive Fe pool is defined as Fe contained in silicate minerals after removal of reactive phases (near boiling 6 N HCl extractable Fe). Total Fe was obtained by summing up the highly reactive Fe pools and the non-reactive Fe contained in silicate minerals (Fig. S-1). The entire procedure is detailed in (Friese *et al*., 2021).

Pore water sampling and geochemical analyses

Pore water within the upper 10 m of TDP-1A cores was extracted using Rhizon Pore Water Samplers (Rhizosphere research products), directly inserted into the soft sediment. Below 10 m depth, we removed the more compact sediment samples from their liner and scraped off all potentially contaminated rims with a sterile spatula. The remaining sediment was transferred into an IODP-style titanium pore water extraction cylinder and placed on a two-column bench top laboratory hydraulic press (Carver Inc.). Pore water was filtered through a sterile 0.2 µm syringe filter and collected in a glass syringe pre-flushed with nitrogen. For anion analysis, 1 mL of pore water was transferred to a screw neck glass vial (VWR International) and stored at 4 °C until analysis. Alkalinity, pH, and Fe^{2+} concentrations were determined in the field *via* colourimetric titration, potentiometry and spectrophotometry, respectively. Major ions were analysed at GFZ Potsdam by ion chromatography.

The pH was measured in the field with a portable pH metre (Thermo Scientific Orion, Star A321) calibrated at pH = 4, 7 and 10. We homogenised 2 mL of sediment in 2 mL of deionised water and measured the supernatant after 2 min and calibrated our results based on standard reference materials, as commonly done for organic-rich soil samples (Black, 1973). Total alkalinity was measured *via* colourimetric titration on pore water samples. Dissolved inorganic carbon (DIC) concentrations were calculated by solving the carbonate system using the pH and alkalinity profiles and borehole temperatures (Jenkins and Moore, 1977). Dissolved Fe^{2+} concentrations were measured directly after pore water retrieval using 1 mL aliquots transferred to 1.6 mL Rotilabo single-use cells (Carl Roth) and stabilised by adding 100 µL of Ferrozine Iron Reagent (Sigma-Aldrich Chemie). Absorbance of the coloured solution was measured at 562 nm with a DR 3900 spectrophotometre (Hach). To determine pore water total Fe concentrations, 150 µL of hydroxylamine hydrochloride were added to 800 µL of the previous mixture, left to react 10 min to reduce all dissolved Fe^{3+}, stabilised by adding 50 µL ammonium acetate and absorbance of the solution measured a second time (Viollier *et al*., 2000). Pore water total Fe concentrations were found to be the same as Fe^{2+} concentrations, and thus Fe^{3+} is absent in pore water. Detection limit of the method is 0.25 µM. Concentrations of Mn^{2+} were analysed *via* spectrophotometry as previously published (Jones *et al*., 2011), following the formaldoxime method (Brewer and Spencer, 1971). Concentrations of PO_4^{3-} in pore water were measured in the field by spectrophotometry. We aliquoted 0.5 mL pore water to 1.5 mL disposable cuvettes (Brand Gmbh) and added 80 µL colour reagent consisting of ammonium molybdate containing ascorbic acid and antimony. Absorbance was measured at 882 nm with a DR 3900 spectrophotometre (Hach). Detection limit of the method is 0.05 µM. Pore water Ca^{2+}, Mg^{2+}, SO_4^{2-} and NH_4^+ concentrations were analysed by normal and suppressed ion chromatography. Based on signal-to-noise ratios of 3 and 10, respective detection and quantification limits of the method calibrated on a multi-element standard are 8.3 and 38.5 µM for Ca^{2+}, 9.6 and 44.6 µM for Mg^{2+}, 2.0 and 8.4 µM for SO_4^{2-}, and 11.3 and 67.6 µM for NH_4^+. All samples were measured in triplicates, with reproducibility better than 5 %. All procedures were previously published (Vuillemin *et al*., 2016, 2023).

The concentrations of trace metals in pore water (*i.e.* As, Co) were measured *via* inductively coupled plasma mass spectrometry (ICP-MS). For this purpose, 100 µL of pore water sample were added to 10 mL of HNO_3 2 % with 10 µL of standard solution, mixed thoroughly, and then measured using a ThermoFischer HR-ICP-MS system. Concentrations of trace elements in pore water were calculated based on the standard spiked in the sample.

Concentrations of formate, lactate, acetate, butyrate and propionate in the pore water were measured by 2-dimensional ion chromatography mass spectrometry (2D IC-MS) (Glombitza *et al*., 2014). Measurements were performed with a Dionex ICS3000 ion chromatograph coupled to a Surveyor MSQ Plus mass spectrometre (both Thermo Scientific). The first chromatograph dimension separates the volatile fatty acids (VFAs) from other inorganic ions by trapping them on a concentrator column and subsequently separating them in the second chromatography dimension. Prior to analysis, pore water samples were filtered through disposable syringe filters (Acrodisc 13 mm IC, pore size 0.2 µm) rinsed with 10 mL ultrapure Milli-Q water directly before use. The first 0.5 mL of filtered pore water was discarded and the second 0.5 mL used for analysis. Quantification was achieved by a three-point calibration with external standards containing a mixture of the analysed VFAs at different concentrations (*i.e.* 200, 500 and 800 µg L^{-1}). Detection limits for formate and acetate were 0.37 and 0.19 µM, respectively. For methane analysis, 2 cm^3 of sediment were transferred on site inside the anaerobic chamber with a cut-off syringe to a 20 mL crimp vial filled with saturated NaCl solution and stored at 4 °C. For analysis, 3 mL helium (He) was introduced to form a headspace followed by 12 h equilibration. Methane concentration was determined by injecting 200 µL of the He headspace into a Thermo Finnigan Trace gas chromatograph (Thermo Fisher Scientific) equipped with a flame ionisation detector (Heuer *et al*., 2009).

Potential sulfate reduction rates (pSRRs) were determined by sediment incubation (Kallmeyer *et al*., 2004) with radioactive $^{35}SO_4^{2-}$ using sterile glass plug mini-cores processed in triplicates (Friese *et al*., 2021). The microbially reduced inorganic sulfur species were separated using a cold chromium distillation (Kallmeyer *et al*., 2004) and radioactivity in the extracts quantified using Ultima Gold Scintillation Cocktail (Perkin Elmer, Waltham) and a Tri-Carb 2500 TR liquid scintillation counter (Packard Instruments).

XRF core-scanning elemental profiles on bulk sediment

All cores used in the splice composite sequence covering the upper 100 m of sediments recovered from TDP Site 1 (106 split-core sections) were scanned on a XRF core scanner (ITRAX, Cox Ltd., Sweden) equipped with a chromium anode X-ray tube (Cr-tube) set to 30 kV, 50 mA and 50 s integration time at 5 mm resolution. Measurements were repeated with a molybdenum anode X-ray tube (Mo-tube) with the same settings to resolve elements with high atomic numbers (Morlock *et al*., 2021).

Sporadic event layers (tephra and turbidites) as well as intervals with low XRF performance and gaps related to uneven core surfaces were removed from the dataset during post-processing. The dataset was mathematically corrected *via* a multivariate log-ratio calibration (MCL) algorithm and data transformation (Weltje and Tjallingi, 2008) on the ItraXelerate software v. 2.4 (Bloemsma *et al*., 2012). This correction allows for the estimation of values in weight % [wt. %] for all elements measured through XRF.

Mineral extraction and SEM imaging

In the field, core catchers were packed into gas-tight aluminum foil bags flushed with nitrogen gas and heat-sealed to keep them under anoxic conditions until mineral extraction. Minerals from core catcher sediments were extracted after 3 months of storage, whereas siderite and vivianite crystals from split TDP-1A cores were extracted from sediment beds with macroscopic enrichment in these phases after 8 months of storage at LacCore. Siderite, millerite and vivianite crystals were retrieved *via* density separation and sorted by placing a neodymium magnet under the beaker and rinsing out the non-magnetic fraction with deionised water (Vuillemin *et al*., 2019a).

Morphological investigation and elemental analysis of the dense mineral fractions obtained from a volume of 50 mL of sediment were processed *via* scanning electron microscopy (SEM) coupled to energy dispersive X-ray spectroscopy (EDX). The samples were prepared by putting an extract of dense minerals or macroscopic crystals onto carbon coated disc which was glued onto SEM aluminum stubs. The samples were carbon coated (~20 nm layer) using a Leica EM ACE600 high-vacuum sputter coater. SEM analysis was performed on a Zeiss Ultra 55 Plus field SEM (for siderites) and on a FEI Quanta 3D FEG (for millerites) at a voltage of 20 kV acceleration voltage. Elemental composition of the imaged samples was determined based on SEM-EDX point and area analyses *via* Octane Elect detector from EDAX (Ametek Inc.). EDX data analysis and acquisition was performed on the EDAX-APEX EDX interface software (Ametek Inc.).

Data accessibility

The present scientific data are archived and publicly available from the PANGAEA® Data Publisher for Earth and Environmental Science (datasets #908080 and #934401) (Vuillemin *et al*., 2019b, 2021).

Supplementary Figures

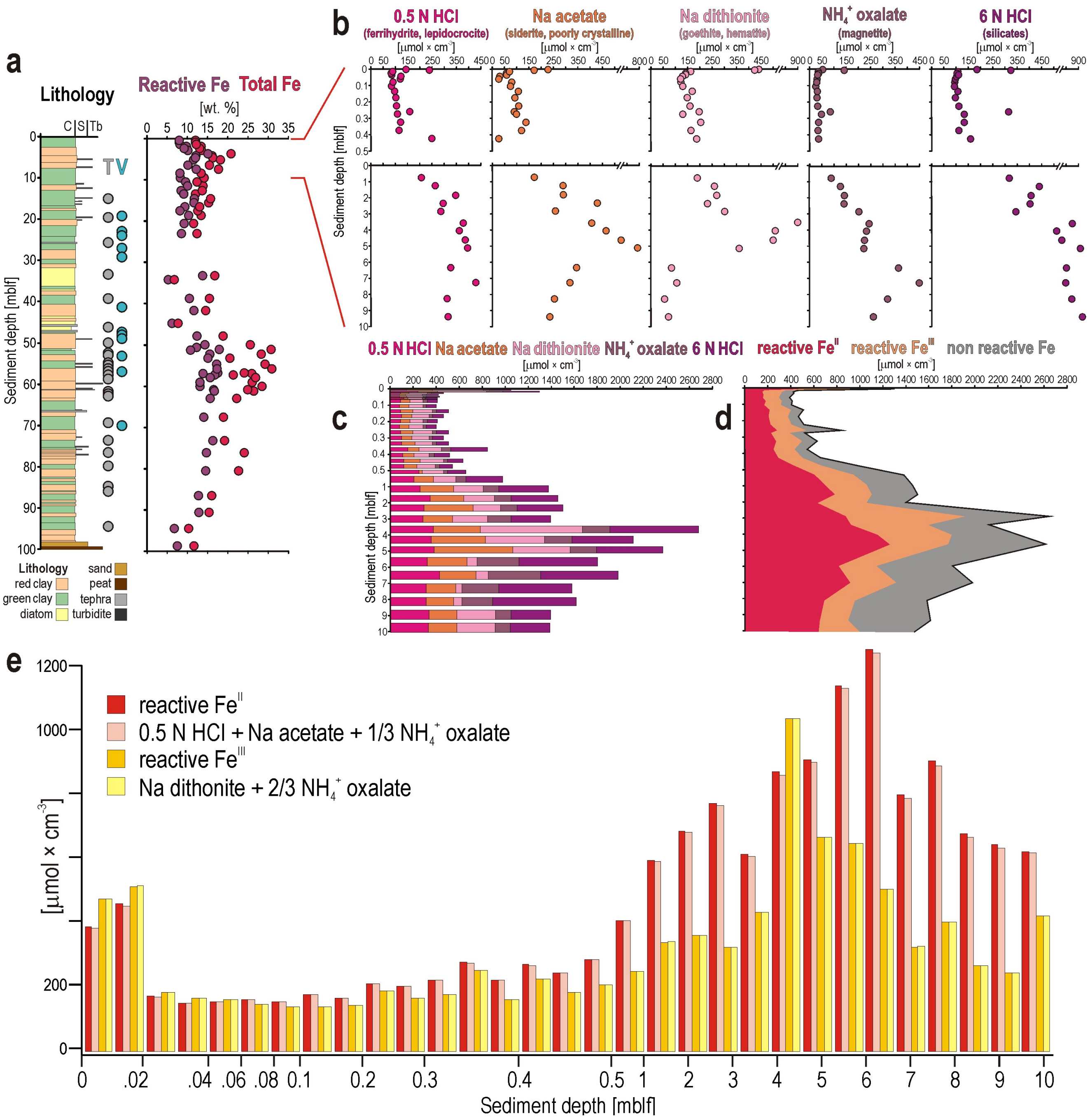

Figure S-1 Additional depth profiles for bulk iron and sequentially extracted iron phases. **(a)** Stratigraphy of site TDP-1A and reactive and total iron. **(b)** Separate and **(c)** cumulative plots for iron fractions sequentially extracted with solutions of 0.5 N HCl, sodium acetate adjusted to pH 4.5, sodium dithionite adjusted to pH 4.8, 0.2 M ammonium oxalate with 0.17 M oxalic acid adjusted to pH 3.2, and near boiling 6 N HCl. **(d)** Iron speciation was determined spectrophotometically. Note that Fe^{III} within the 0.5 N HCl fraction was below detection, so that the reactive Fe^{III} pool is entirely composed of the sodium dithionite (*e.g.*, goethite, hematite) and ammonium oxalate (*e.g.*, magnetite) fractions. **(e)** Close-up of the cumulative plot for sequentially extracted iron fractions (modified from Friese *et al.*, 2021).

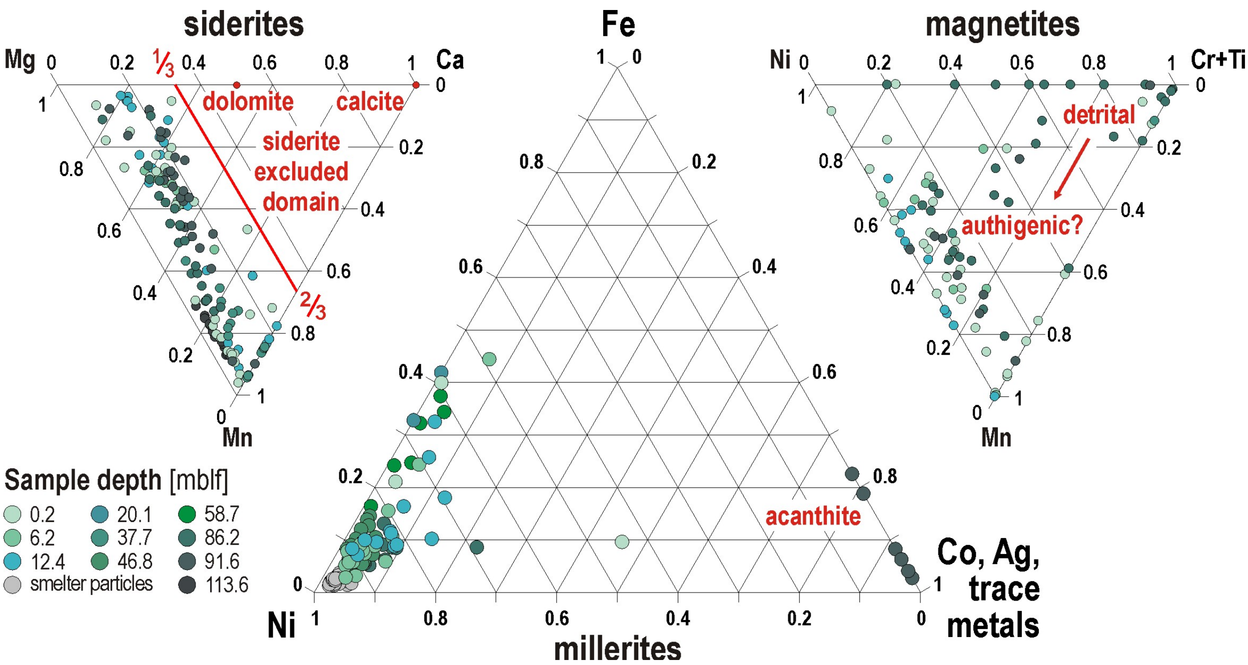

Figure S-2 Elemental EDX point analyses. The ternary plots show that millerites include minor Fe^{2+} traces **(centre)**. Acanthite (ac) was also identified in deep sediments (see Fig. S-8). Siderites **(left)** substitute Mn^{2+} for Fe^{2+} in the initial growth phase, incorporating variable amount of Mg^{2+} but constant Ca^{2+} traces in crystal rims. Magnetites **(right)** show some indication of trace metal incorporation related to microbial reduction. Although trace elements (*e.g.*, Ni, Mn, Ti and Cr) are common in magmatic magnetites, increased Mn and Ni contents potentially point to neoformation of magnetites in the water column (Bauer *et al.*, 2020) and sediment (Vuillemin *et al.*, 2019a).

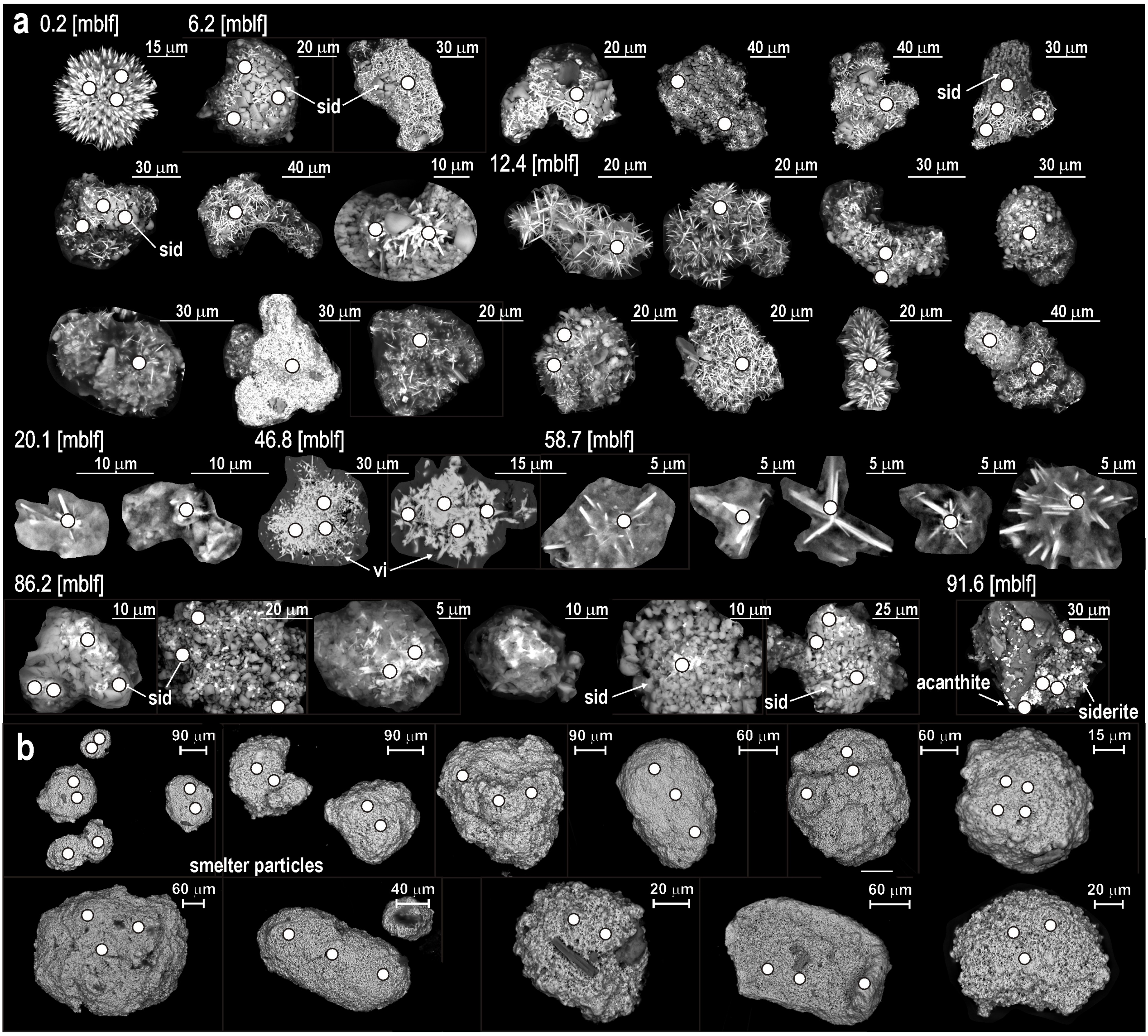

Figure S-3 SEM images of millerites and corresponding points of EDX analyses. **(a)** Millerite crystals identified in dense fractions, sometime entangled with siderite or as inclusions in vivianites, and corresponding points of EDX analyses. Acanthite was identified in a sample from 91.6 mblf (see Fig. S-8). **(b)** Millerite dust contaminants (*i.e.* smelter particles) derived from Sorowako's nickel mine smelter and corresponding points of EDX analyses.

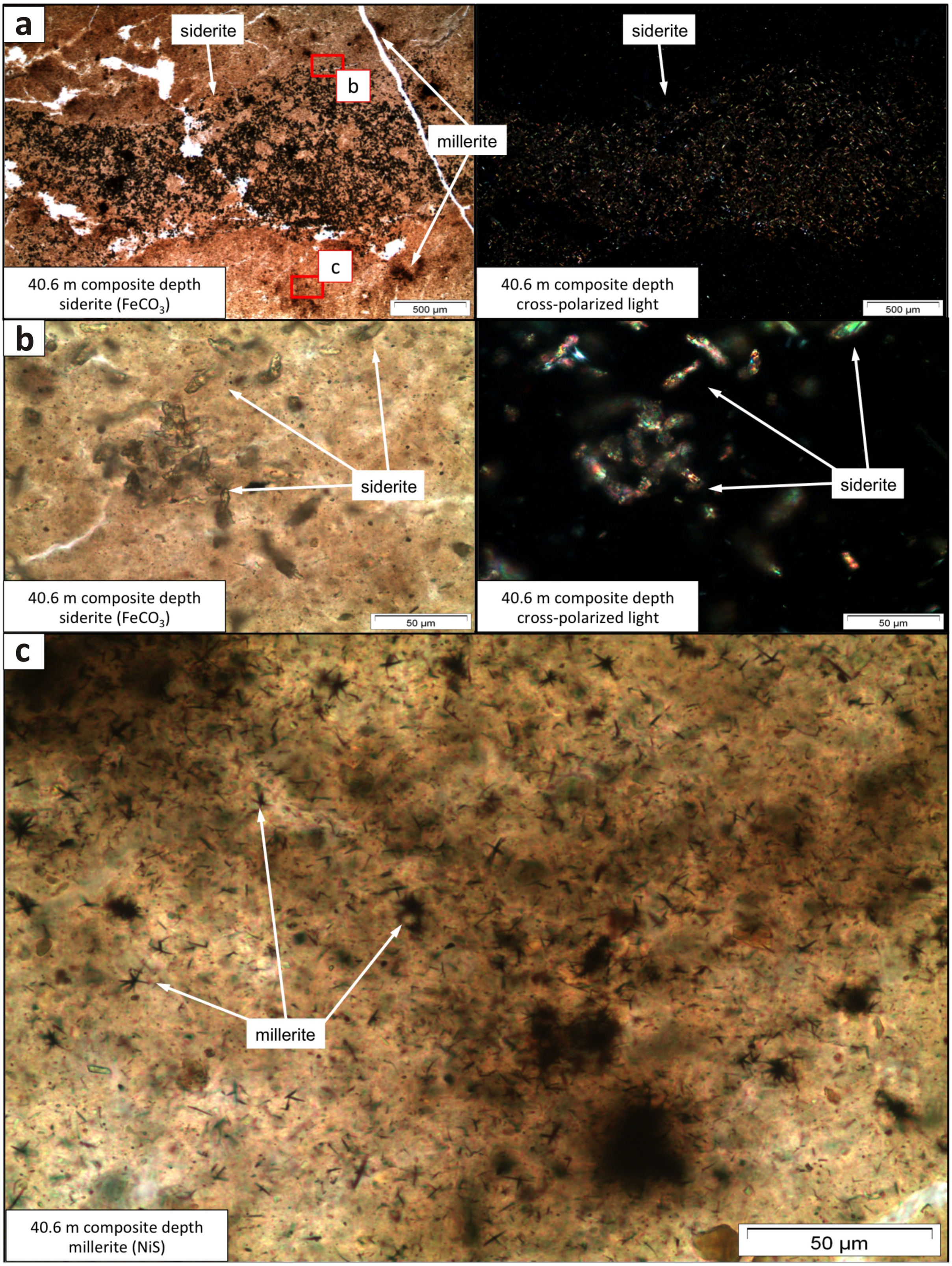

Figure S-4 Optical images of sediment smear slides in natural and polarised light. The density of siderite and millerite crystals in the vicinity of micro-cracks in the sediment argue for secondary precipitation from pore water associated with the additional pore space accommodated during seismic events with **(a–c)** close-ups to millerite crystals.

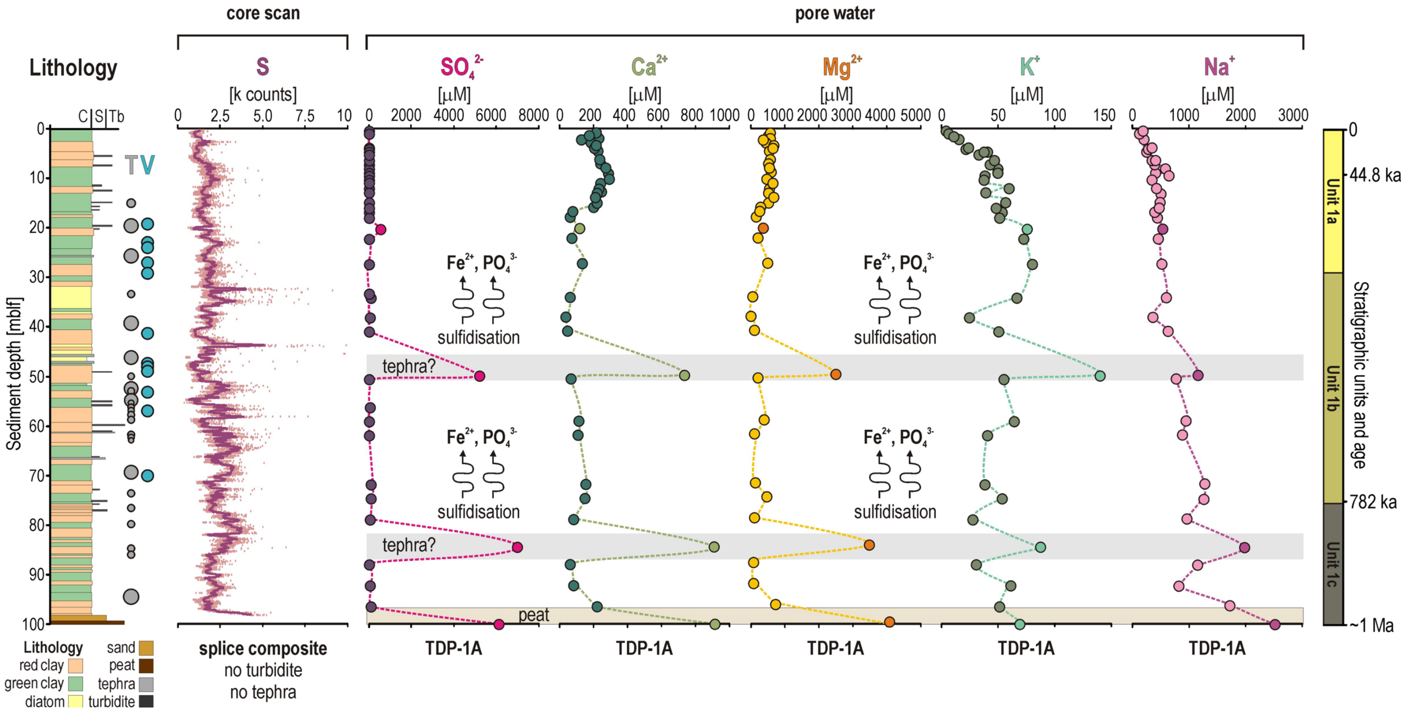

Figure S-5 Depth profiles for bulk sediment, and pore water geochemistry. **(Left to right)** Stratigraphy of site TDP-1A; XRF core-scanning profile for total S; pore water concentrations for SO_4^{2-}, Ca^{2+}, Mg^{2+}, K^+ and Na^+. The outliers in pore water concentrations may be explained by sporadic tephra and dissolution of anhydrite ($CaSO_4$) and sanidine ($KAlSi_3O_8$). An additional source of sulfate to the lake could result in sulfidisation of iron oxides (*e.g.*, goethite, hematite) with subsequent release and diffusion of pore water Fe^{2+} and PO_4^{3-} that would promote saturated conditions with respect to vivianite. Similarly, microbial acid-sulfate weathering of basaltic tephra could (trans)form ferric minerals, *e.g.*, jarosite [(K, Na, $H_3O)Fe^{3+}{}_3(SO_4)_2(OH)_6$], to release sulfate (Sekerci and Balci, 2022). Stratigraphic units correspond to: **(Unit 1c)** lake initial stage with basin subsidence and regular riverine-deltaic inflows; **(Unit 1b)** a productive phase with low sedimentation rates; and **(Unit 1a)** hydrological changes and lake level fluctuations during the Late Pleistocene (Russell *et al*., 2020; Vuillemin *et al*., 2023).

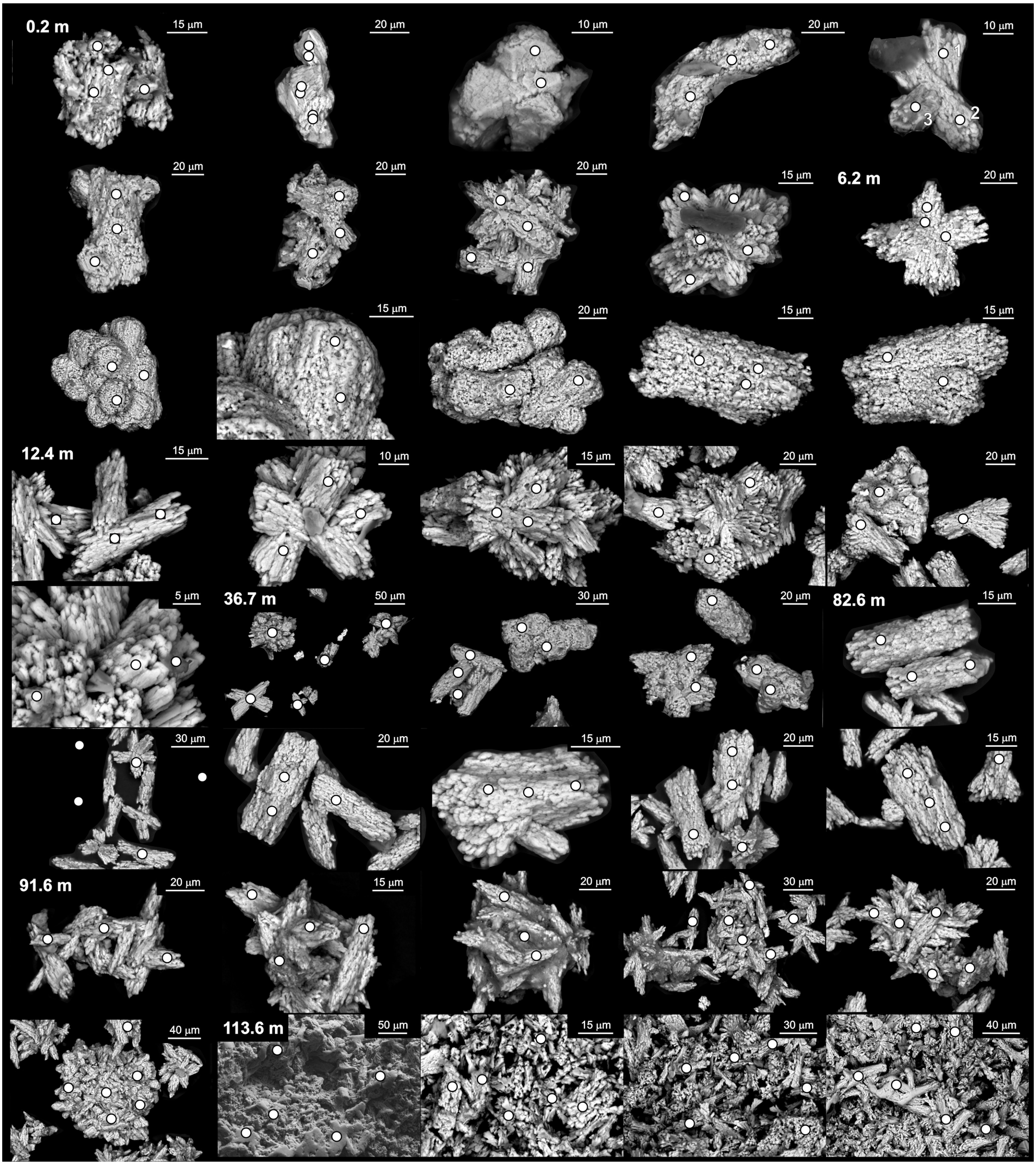

Figure S-6 SEM images of siderites and corresponding points of EDX analyses.

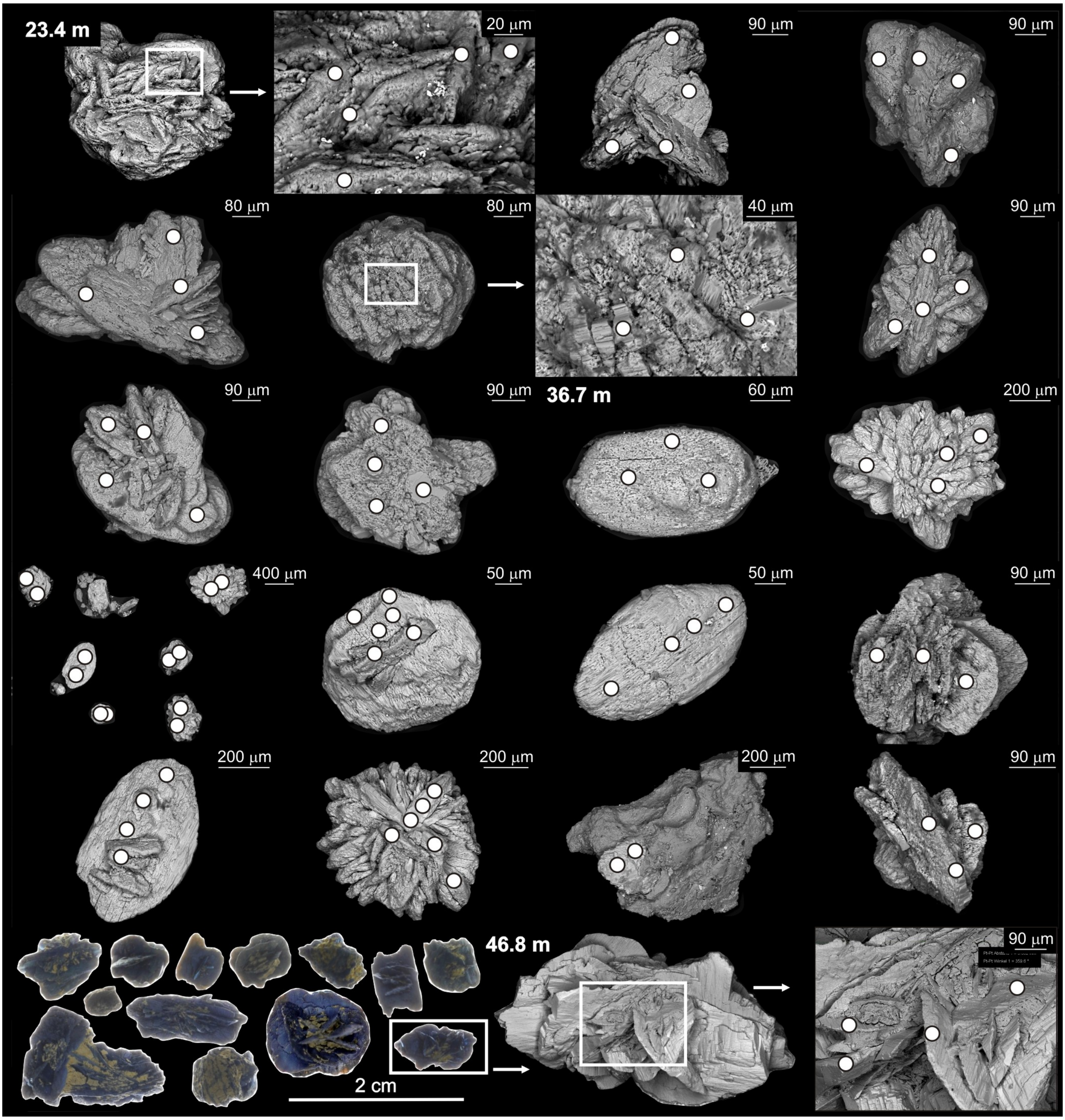

Figure S-7 SEM images of vivianites and corresponding points of EDX analyses.

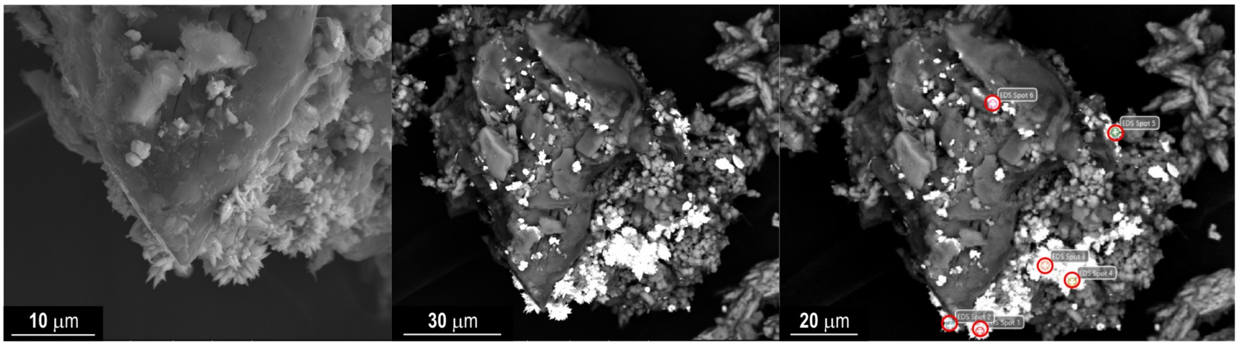

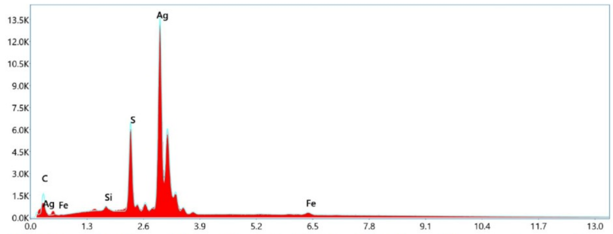

Element	Weight %	MDL	Atomic %	Net Int.	Error %	R	A	F
C K	13.6	0.58	52.0	470.1	12.4	0.7458	0.0897	1.0000
Si K	0.4	0.09	0.7	240.3	13.5	0.7972	0.4811	1.0202
S K	10.0	0.09	**14.4**	5722.3	4.9	0.8087	0.6786	1.0377
Fe K	1.1	0.29	0.9	214.5	17.9	0.8660	0.8709	1.0630
Ag L	74.9	0.29	**32.0**	13880.4	3.6	0.8233	0.7691	1.0038

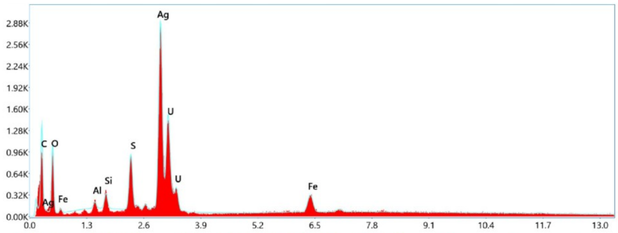

Element	Weight %	MDL	Atomic %	Net Int.	Error %	R	A	F
C K	33.2	0.64	59.1	695.9	11.1	0.8393	0.1274	1.0000
O K	22.0	0.55	29.5	606.9	12.3	0.8535	0.0652	1.0000
Al K	0.4	0.13	0.3	77.0	20.6	0.8806	0.4314	1.0088
Si K	0.7	0.12	0.5	184.9	11.1	0.8854	0.5504	1.0133
S K	3.0	0.10	**2.0**	771.7	5.6	0.8944	0.7379	1.0276
Fe K	4.1	0.37	1.6	365.3	7.9	0.9342	0.9311	1.0667
Ag L	34.0	0.31	**6.7**	2921.5	3.5	0.9054	0.8436	1.0047
U M	2.7	1.38	0.2	191.8	9.6	0.9081	0.8582	1.0176

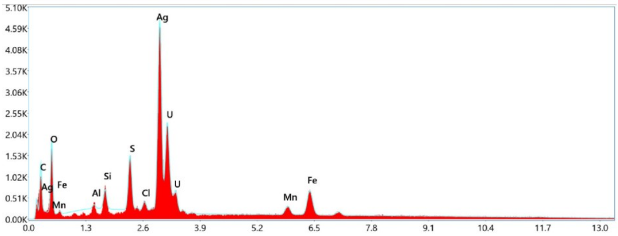

Element	Weight %	MDL	Atomic %	Net Int.	Error %	R	A	F
C K	23.3	0.72	47.2	635.1	11.7	0.8258	0.1114	1.0000
O K	24.1	0.55	36.7	1045.5	11.5	0.8403	0.0689	1.0000
Al K	0.3	0.13	0.2	78.4	23.3	0.8686	0.4056	1.0092
Si K	1.0	0.12	0.9	382.8	9.1	0.8736	0.5256	1.0140
S K	3.3	0.10	**2.5**	1235.8	5.8	0.8831	0.7176	1.0295
Cl K	0.1	0.14	0.1	41.4	61.8	0.8876	0.7669	1.0448
Mn K	2.0	0.29	0.9	285.2	12.3	0.9215	0.9071	1.0582
Fe K	6.4	0.36	2.8	834.0	5.3	0.9257	0.9255	1.0604
Ag L	38.2	0.31	**8.6**	4808.8	3.5	0.8947	0.8293	1.0049
U M	1.3	1.03	0.1	130.7	16.7	0.8977	0.8453	1.0219

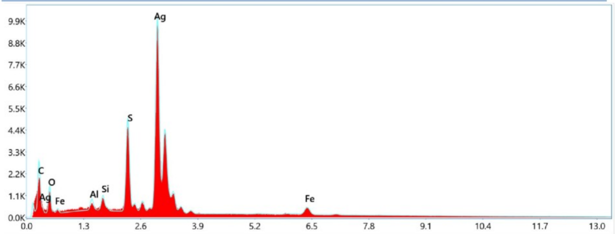

Element	Weight %	MDL	Atomic %	Net Int.	Error %	R	A	F
C K	28.7	0.52	60.2	1246.1	11.1	0.8152	0.1003	1.0000
O K	13.2	0.44	20.9	822.5	12.3	0.8299	0.0559	1.0000
Al K	0.8	0.08	0.8	447.7	10.9	0.8589	0.4212	1.0113
Si K	0.9	0.07	0.8	618.0	8.1	0.8641	0.5360	1.0174
S K	6.6	0.07	**5.2**	4471.7	4.5	0.8739	0.7240	1.0334
Fe K	2.2	0.20	1.0	513.0	9.4	0.9187	0.9142	1.0647
Ag L	47.5	0.21	**11.1**	10438.0	3.2	0.8860	0.8166	1.0039

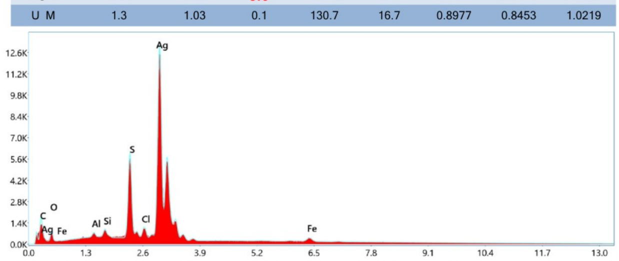

Element	Weight %	MDL	Atomic %	Net Int.	Error %	R	A	F
C K	17.0	0.58	50.5	657.2	12.0	0.7724	0.0915	1.0000
O K	7.3	0.49	16.2	395.7	13.2	0.7872	0.0502	1.0000
Al K	0.5	0.10	0.6	235.8	15.6	0.8181	0.3840	1.0122
Si K	0.7	0.08	0.9	420.4	10.4	0.8238	0.4986	1.0190
S K	8.3	0.08	**9.2**	5243.6	4.8	0.8348	0.6933	1.0365
Cl K	0.5	0.13	0.5	280.6	16.2	0.8401	0.7188	1.0552
Fe K	1.5	0.26	0.9	319.3	15.8	0.8876	0.8873	1.0635
Ag L	64.3	0.26	**21.2**	13268.3	3.5	0.8486	0.7854	1.0038

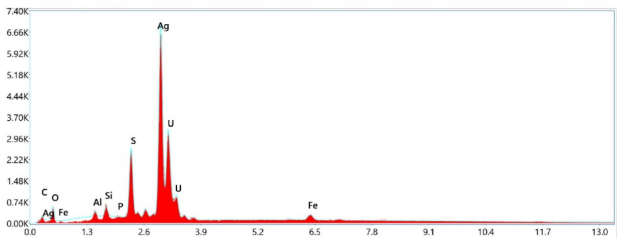

Element	Weight %	MDL	Atomic %	Net Int.	Error %	R	A	F
C K	4.4	0.77	18.1	87.7	17.4	0.7429	0.0947	1.0000
O K	10.5	0.66	32.4	295.5	13.5	0.7572	0.0521	1.0000
Al K	0.6	0.16	1.1	128.1	17.8	0.7884	0.3517	1.0109
Si K	1.0	0.14	1.8	287.4	11.5	0.7943	0.4631	1.0166
P K	0.0	0.10	0.1	8.9	73.8	0.8002	0.5652	1.0263
S K	7.6	0.13	**11.7**	2276.0	5.5	0.8059	0.6601	1.0322
Fe K	2.4	0.42	2.2	265.2	13.6	0.8636	0.8705	1.0640
Ag L	69.7	0.39	**32.0**	7036.8	3.8	0.8205	0.7683	1.0041
U M	3.8	1.60	0.8	318.8	11.6	0.8244	0.7848	1.0169

Figure S-8 SEM images of acanthite and corresponding points of EDX analyses.

Supplementary Table

Table S-1 Modelled saturation indices based on pH, alkalinity, pore water concentrations of major ions and borehole temperatures.

SUPPLEMENTARY TABLE S-1. MODELLED SATURATION INDICES

5 m: zone 1	Saturation	10 m: zone 2	Saturation	35 m: zone 4	Saturation
talc/serpentine	**1.43**	**siderite**	**1.00**	**siderite**	**1.00**
siderite	**1.29**	quartz	0.71	quartz	0.71
quartz	0.71	chalcedony	0.29	chalcedony	0.29
chalcedony	0.29	**vivianite**	**-0.04**	**vivianite**	**-0.04**
vivianite	**-0.45**	**talc/serpentine**	**-0.31**	**talc/serpentine**	**-0.31**
α SiO_2	-0.54	α SiO_2	-0.54	α SiO_2	-0.54
calcite	-0.68	calcite	-0.83	calcite	-0.83
dolomite	-0.77	aragonite	-0.97	aragonite	-0.97
aragonite	-0.82	dolomite	-1.27	dolomite	-1.27

Supplementary Information References

Bauer, K.W., Byrne, J.M., Kenward, P., Simister, R.L., Michiels, C.C., Friese, A., Vuillemin, A., Henny, C., Nomosatryo, S., Kallmeyer, J., Kappler, A., Smit, M.A., Francois, R., Crowe, S.A. (2020) Magnetite biomineralization in ferruginous waters and early Earth evolution. *Earth and Planetary Science Letters* 549, 116495. https://doi.org/10.1016/j.epsl.2020.116495

Black, C.A. (1973) Methods of soil analysis: test methods for evaluating solid waste. In: *Physical/Chemical Methods, 9045B Soil and Waste pH*. American Society of Agronomy, Madison, USA. https://www.epa.gov/hw-sw846/sw-846-test-method-9045d-soil-and-waste-ph

Bloemsma, M.R., Zabel, M., Stuut, J.B.W., Tjallingii, R., Collins, J.A., Weltje, G.J. (2012) Modelling the joint variability of grain size and chemical composition in sediments. *Sedimentary Geology* 280, 135–148. https://doi.org/10.1016/j.sedgeo.2012.04.009

Brewer, P.G., Spencer, D.W. (1971) Colorimetric determination of manganese in anoxic waters. *Limnology and Oceanography* 16, 107–110. https://doi.org/10.4319/lo.1971.16.1.0107

Friese, A., Kallmeyer, J., Kitte, J.A., Montaño Martínez, I., Bijaksana, S., Wagner, D., the ICDP Lake Chalco Drilling Science Team, the ICDP Towuti Drilling Science Team (2017) A simple and inexpensive technique for assessing contamination during drilling operations. *Limnology and Oceanography: Methods* 15, 200–211. https://doi.org/10.1002/lom3.10159

Friese, A., Bauer, K., Glombitza, C., Ordoñez, L., Ariztegui, D., Heuer, V.B., Vuillemin, A., Henny, C., Nomosatryo, S., Simister, R., Wagner, D., Bijaksana, S., Vogel, H., Melles, M., Russell, J.M., Crowe, S.A., Kallmeyer, J. (2021) Organic matter mineralization in modern and ancient ferruginous sediments. *Nature Communications* 12, 2216. https://doi.org/10.1038/s41467-021-22453-0

Henkel, S., Kasten, S., Hartmann, J.F., Silva-Busso, A., Staubwasser, M. (2018) Iron cycling and stable Fe isotope fractionation in Antarctic shelf sediments, King George Island. *Geochimica et Cosmochimica Acta* 237, 320–338. https://doi.org/10.1016/j.gca.2018.06.042

Heuer, V.B., Pohlman, J.W., Torres, M.E., Elvert, M., Hinrichs, K.-U. (2009) The stable carbon isotope biogeochemistry of acetate and other dissolved carbon species in deep subseafloor sediments at the northern Cascadia Margin. *Geochimica et Cosmochimica Acta* 73, 3323–3336. https://doi.org/10.1016/j.gca.2009.03.001

Glombitza, C., Pedersen, J., Røy, H., Jørgensen, B.B. (2014) Direct analysis of volatile fatty acids in marine sediment porewater by two-dimensional ion chromatography-mass spectrometry. *Limnology and Oceanography: Methods* 12, 455–468. https://doi.org/10.4319/lom.2014.12.455

Jenkins, S.R., Moore, R.C. (1977) A Proposed Modification to the Classical Method of Calculating Alkalinity in Natural Waters. *Journal AWWA* 69, 56–60. https://doi.org/10.1002/j.1551-8833.1977.tb02544.x

Jones, C., Crowe, S.A., Sturm, A., Leslie, K.L., MacLean, L.C.W., Katsev, S., Henny, C., Fowle, D.A., Canfield, D.E. (2011) Biogeochemistry of manganese in ferruginous Lake Matano, Indonesia. *Biogeosciences* 8, 2977–2991. https://doi.org/10.5194/bg-8-2977-2011

Kallmeyer, J., Ferdelman, T.G., Weber, A., Fossing, H., Jørgensen, B.B. (2004) A cold chromium distillation procedure for radiolabeled sulfide applied to sulfate reduction measurements. *Limnology and Oceanography: Methods* 2, 171–180. https://doi.org/10.4319/lom.2004.2.171

Morlock, M.A., Vogel, H., Russell, J.M., Anselmetti, F.S., Bijaksana, S. (2021) Quaternary environmental changes in tropical Lake Towuti, Indonesia, inferred from end-member modelling of X-ray fluorescence core-scanning data. *Journal of Quaternary Science* 36, 1040–1051. https://doi.org/10.1002/jqs.3338

Ordoñez, L., Vogel, H., Sebag, D., Ariztegui, D., Adatte, T., Russell, J.M., Kallmeyer, J., Vuillemin, A., Friese, A., Crowe, S.A., Bauer, K.W., Simister, R., Henny, C., Nomosatryo, S., Bijaksana, S., the Towuti Drilling Project Scientific Team (2019) Empowering conventional Rock-Eval pyrolysis for organic matter characterization of the siderite-rich sediments of Lake Towuti (Indonesia) using End-Member Analysis. *Organic Geochemistry* 134, 32–44. https://doi.org/10.1016/j.orggeochem.2019.05.002

Poulton, S.W., Canfield, D.E. (2005) Development of a sequential extraction procedure for iron: implications for iron partitioning in continentally derived particulates. *Chemical Geology* 214, 209–221. https://doi.org/10.1016/j.chemgeo.2004.09.003

Russell, J.M., Bijaksana, S., Vogel, H., Melles, M., Kallmeyer, J., Ariztegui, D., Crowe, S.A., Fajar, S., Hafidz, A., Haffner, D., Hasberg, A., Ivory, S., Kelly, C., King, J., Kirana, K., Morlock, M., Noren, A., O'Grady, R., Ordonez, L., Stevenson, J., von Rintelen, T., Vuillemin, A., Watkinson, I., Wattrus, N., Wicaksono, S., Wonik, T., Bauer, K., Deino, A., Friese, A., Henny, C., Imran, Marwoto, R., Ngkoimani, L.O., Nomosatryo, S., Safiuddin, L.O., Simister, R., Tamuntuan, G. (2016) The Towuti Drilling Project: paleoenvironments, biological evolution, and geomicrobiology of a tropical Pacific lake. *Scientific Drilling* 21, 29–40. https://doi.org/10.5194/sd-21-29-2016

Russell, J.M., Vogel, H., Bijaksana, S., Melles, M., Deino, A., Hafidz, A., Haffner, D., Hasberg, A.K.M., Morlock, M., von Rintelen, T., Sheppard, R., Stelbrink, B., Stevenson, J. (2020) The late quaternary tectonic, biogeochemical, and environmental evolution of ferruginous Lake Towuti, Indonesia. *Palaeogeography, Palaeoclimatology, Palaeoecology* 556, 109905. https://doi.org/10.1016/j.palaeo.2020.109905

Sekerci, F., Balci, N. (2022) Microbial Acid Sulfate Weathering of Basaltic Rocks: Implication for Enzymatic Reactions. *Aquatic Geochemistry* 28, 155–184. https://doi.org/10.1007/s10498-022-09407-8

Viollier, E., Inglett, P.W., Hunter, K., Roychoudhury, A.N., Van Cappellen, P. (2000) The ferrozine method revisited: Fe(II)/Fe(III) determination in natural waters. *Applied Geochemistry* 15, 785–790. https://doi.org/10.1016/S0883-2927(99)00097-9

Vuillemin, A., Friese, A., Alawi, M., Henny, C., Nomosatryo, S., Wagner, D., Crowe, S.A., Kallmeyer, J. (2016) Geomicrobiological Features of Ferruginous Sediments from Lake Towuti, Indonesia. *Frontiers in Microbiology* 7, 1007. https://doi.org/10.3389/fmicb.2016.01007

Vuillemin, A., Wirth, R., Kemnitz, H., Schleicher, A.M., Friese, A., Bauer, K.W., Simister, R., Nomosatryo, S., Ordoñez, L., Ariztegui, D., Henny, C., Crowe, S.A., Benning, L.G., Kallmeyer, J., Russell, J.M., Bijaksana, S., Vogel, H., the Towuti Drilling Project Science Team (2019a) Formation of diagenetic siderite in modern ferruginous sediments. *Geology* 47, 540–544. https://doi.org/10.1130/G46100.1

Vuillemin, A. Friese, A., Lücke, A., Bauer, K.W., Nomosatryo, S., Simister, R., Ordoñez, L.G., Ariztegui, D., Russell, J.M., Bijaksana, S., Vogel, H., Crowe, S.A., Kallmeyer, J., the Towuti Drilling Project Science Team (2019b) Pore water geochemistry and bulk sediment measurements of downcore profiles from site TDP-1A of the ICDP Towuti Drilling Project, Lake Towuti, Indonesia. *PANGAEA*. https://doi.pangaea.de/10.1594/PANGAEA.908080

Vuillemin, A., Mayr, C., Friese, A., Bauer, K.W., Lücke, A., Heuer, V.B., Glombitza, C., Henny, C., von Blanckenburg, F., Russell, J.M., Bijaksana, S., Vogel, H., Crowe, S.A., Kallmeyer, J. (2021) Siderite C-O-Fe isotope compositions, pore water geochemistry and bulk sediment parameters from the 100-m-long core TDP-1A of the ICDP Towuti Drilling Project, Lake Towuti, Indonesia. *PANGAEA*. https://doi.pangaea.de/10.1594/PANGAEA.934401

Vuillemin, A., Mayr, C., Schuessler, J.A., Friese, A., Bauer, K.W., Lücke, A., Heuer, V.B., Glombitza, C., Henny, C., von Blanckenburg, F., Russell, J.M., Bijaksana, S., Vogel, H., Crowe, S.A., Kallmeyer, J. (2023) A one-million-year isotope record from siderites formed in modern ferruginous sediments. *GSA Bulletin* 135, 504–522. https://doi.org/10.1130/B36211.1

Weltje, G.J., Tjallingii, R. (2008) Calibration of XRF core scanners for quantitative geochemical logging of sediment cores: Theory and application. *Earth and Planetary Science Letters* 274, 423–438. https://doi.org/10.1016/j.epsl.2008.07.054